

1 **A recombinant ‘ACE2 Triple Decoy’ that traps and neutralizes SARS-CoV-2**
2 **shows enhanced affinity for highly transmissible SARS-CoV-2 variants**

3
4 Shiho Tanaka^{1*}, Gard Nelson^{1*}, Anders Olson¹, Oleksandr Buzko¹, Wendy Higashide¹, Annie
5 Shin¹, Marcos Gonzales¹, Justin Taft^{2,3}, Roosheel Patel^{2,3}, Sofija Buta^{2,3,4}, Marta Martin-
6 Fernandez^{2,3,4,5,6}, Dusan Bogunovic^{2,3,4,5,6}, Patricia, Spilman¹, Kayvan Niazi¹, Shahrooz
7 Rabizadeh¹, and Patrick Soon-Shiong¹

8
9 *These authors contributed equally

10
11 ¹ImmunityBio, Inc.

12 ²Center for Inborn Errors of Immunity, ³Department of Pediatrics, ⁴Precision Immunology
13 Institute, ⁵Mindich Child Health and Development Institute, ⁶Department of Microbiology, Icahn
14 School of Medicine at Mount Sinai, 1 Gustave Lane, Levy Place, New York, NY 10029-5674,
15 USA SPA

16
17 **Summary sentence**

18 An ACE2(N27Y/H34A/H374N)-IgG₁FC fusion protein decoy sustains high affinity to all
19 SARS-CoV-2 spike receptor binding domain (RBD) protein variants tested, shows enhanced
20 affinity for the N501Y and L452R variants, and the highest affinity for combined N501Y and
21 E484K variants.

22

23

24 **ABSTRACT**

25 The highly-transmissible SARS-CoV-2 variants now replacing the first wave strain pose an
26 increased threat to human health by their ability, in some instances, to escape existing humoral
27 protection conferred by previous infection, neutralizing antibodies, and possibly vaccination.
28 Thus, other therapeutic options are necessary. One such therapeutic option that leverages SARS-
29 CoV-2 initiation of infection by binding of its spike receptor binding domain (S RBD) to surface-
30 expressed host cell angiotensin-converting enzyme 2 (ACE2) is an ACE2 ‘decoy’ that would trap
31 the virus by competitive binding and thus inhibit propagation of infection. Here, we used
32 Molecular Dynamic (MD) simulations to predict ACE2 mutations that might increase its affinity
33 for S RBD and screened these candidates for binding affinity *in vitro*. A double mutant
34 ACE2(T27Y/H34A)-IgG₁F_C fusion protein was found to have very high affinity for S RBD and to
35 show greater neutralization of SARS-CoV-2 in a live virus assay as compared to wild type ACE2.
36 We further modified the double mutant ACE2 decoy by addition of an H374N mutation to inhibit
37 ACE2 enzymatic activity while maintaining high S RBD affinity. We then confirmed the potential
38 efficacy of our ACE2(T27Y/H34A/H374N)-IgG₁F_C Triple Decoy against S RBD expressing
39 variant-associated E484K, K417N, N501Y, and L452R mutations and found that our ACE2 Triple
40 Decoy not only maintains its high affinity for S RBD expressing these mutations, but shows
41 enhanced affinity for S RBD expressing the N501Y or L452R mutations and the highest affinity
42 for S RBD expressing both the E484K and N501Y mutations. The ACE2 Triple Decoy also
43 demonstrates the ability to compete with wild type ACE2 in the cPass™ surrogate virus
44 neutralization in the presence of S RBD with these mutations. Additional MD simulation of ACE2
45 WT and decoy interactions with S RBD WT or B.1.351 variant sequence S RBD provides insight
46 into the enhanced affinity of the ACE2 decoy for S RBD and reveals its potential as a tool to

47 predict affinity and inform therapeutic design. The ACE2 Triple Decoy is now undergoing
48 continued assessment, including expression by a human adenovirus serotype 5 (hAd5) construct
49 to facilitate delivery *in vivo*.

50 INTRODUCTION

51 SARS-CoV-2 variants have rapidly swept the globe ¹⁻³ and very recent investigations reveal
52 that several of these variants have shown the ability to escape neutralization by convalescent
53 antibodies in recovered COVID-19 patients ⁴ and recombinant neutralizing antibodies (nAbs)
54 developed as therapeutics. ^{5,6} There are also fears that current vaccines may not be as effective
55 against some of the variants and early evidence suggests that for some vaccines, this risk may exist.
56 ^{7,8} The latter is a particular concern, as the massive vaccine efforts currently underway employ
57 vaccines designed to elicit immune responses against first-wave sequence SARS-CoV-2 spike (S)
58 protein and specifically the S receptor binding domain (S RBD) that binds to angiotensin-
59 converting enzyme 2 (ACE2) on the surface of human cells in the airway and gut that initiates
60 viral entry and infection. ⁹⁻¹² While one response to the threat of loss of vaccine efficacy might be
61 to continually re-design vaccines to target specific new variants, this would be an ongoing game
62 of catch-up because it can be expected that further novel variants will emerge, particularly since
63 several recent reports have shown that antibodies elicited by infection and vaccination act as
64 evolutionary forces that result in the predominance of viral variants that escape these immune
65 defenses. ^{13,14}

66 While efforts to adapt vaccines should be encouraged, in parallel, new therapeutic approaches
67 to neutralize viral infection that are not undermined by the presence of mutations should be
68 advanced.

69 To address the need for a therapeutic and potentially prophylactic approach that has a low
70 likelihood of being adversely affected by variant mutations, we have designed and tested ACE2
71 ‘decoys’ that leverage the binding of the S RBD to ACE2. This is an approach that is also being
72 pursued by others using a variety of fusion proteins and delivery methods.¹⁵⁻¹⁸ Our ACE2 decoys
73 under development are recombinant ACE2-IgG₁F_C or -IgAF_C fusion proteins, with the ACE2
74 sequence optimized for binding affinity to S RBD. The ACE2 decoy would be given to a patient
75 infected with SARS-CoV-2, act to prevent binding of virus to host cell ACE2 by competing with
76 endogenous ACE2 for spike binding, and allow clearance of the virus.¹⁹⁻²¹

77 To successfully compete, an efficacious ACE2 decoy would ideally have significantly higher
78 affinity for S RBD than endogenous, host-cell expressed ACE2. To identify ACE2 mutations with
79 a high probability of increasing affinity, we utilized our *in silico* Molecular Dynamic (MD)
80 simulation capabilities as described in Nelson *et al.*²² “*Millisecond-scale molecular dynamics*
81 *simulation of spike RBD structure reveals evolutionary adaption of SARS-CoV-2 to stably bind*
82 *ACE2*” wherein we reported on our identification of regions of high affinity interaction between
83 ACE2 and S RBD based on previously reported S RBD structures.^{23,24}

84 Because the ACE2 decoy concept is based on interaction of ACE2 with S RBD, its binding
85 affinity and thus efficacy may also be vulnerable to changes in the SARS-CoV-2 S RBD sequence.
86 We therefore assessed the affinity of our ACE2 decoy, as compared to wild type (WT) ACE2, for
87 S RBD with a variety of single or multiple mutations associated with the currently predominant
88 variants, including the B.1.351 variant expressing E484K, K417N, and N501Y mutations,²⁵ the
89 B.1.1.7 variant (N501Y),^{1,26} and the Cal.20.C L452R variant.²⁷

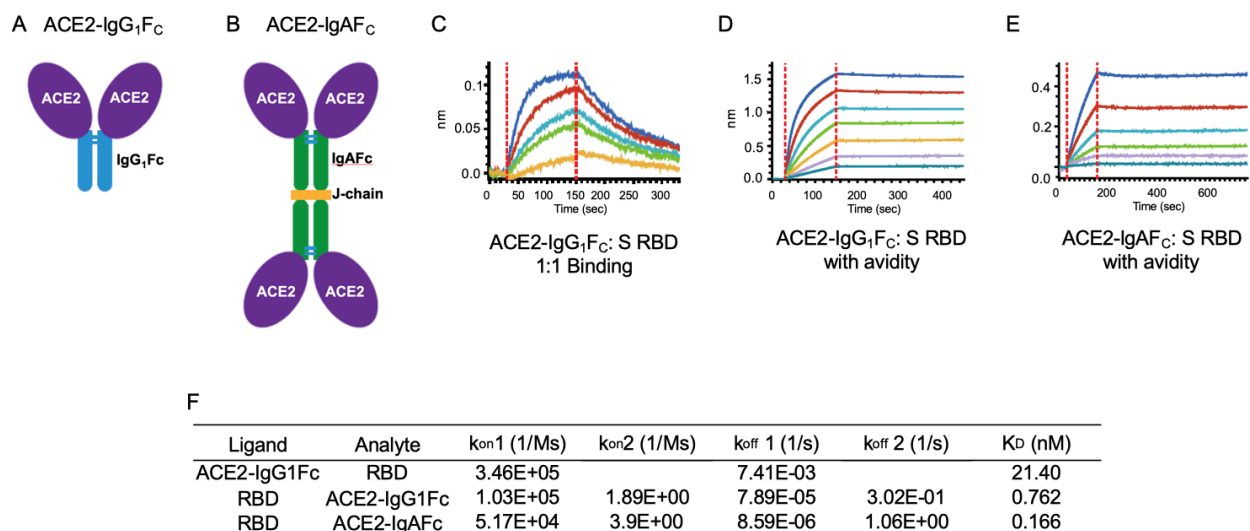
90 Here, we report our findings that the combined N27Y and H34A mutations of ACE2 conferred
91 the greatest increase in affinity for S RBD of the ACE2 variants tested. Our final ACE2 Triple

92 Decoy also included an H374N mutation to abrogate ACE2 enzymatic activity. This ACE2 Triple
 93 Decoy not only maintained affinity for variant S RBD, it showed an increased affinity for S RBD
 94 expressing N501Y or L452R mutations.

95 RESULTS

96 Wild type (WT) ACE2-IgG₁Fc and ACE2-IgAF_C decoys show high affinity for the spike 97 receptor binding domain

98 In initial studies to design an ACE2 decoy, we determined the affinity of both recombinant
 99 wild type (WT) ACE2(WT)-IgG₁Fc and -IgAF_C fusion proteins for binding to S RBD by Bi-layer
 100 Interferometry (BLI) analysis. The ACE2(WT)-IgG₁Fc decoy (Fig. 1A) showed high affinity for
 101 S RBD in both 1:1 binding with a coefficient of dissociation (K_D) of 21.40 nM and binding with
 102 avidity with a K_D of 0.762 nM (Fig. 1C and D, respectively; values in Fig. 1F). The ACE2(WT)-
 103 IgAF_C dimeric fusion protein (Fig. 1B) demonstrated even higher binding (with avidity) affinity
 104 for S RBD with a K_D of 0.166 nM (Fig. 1E and F).



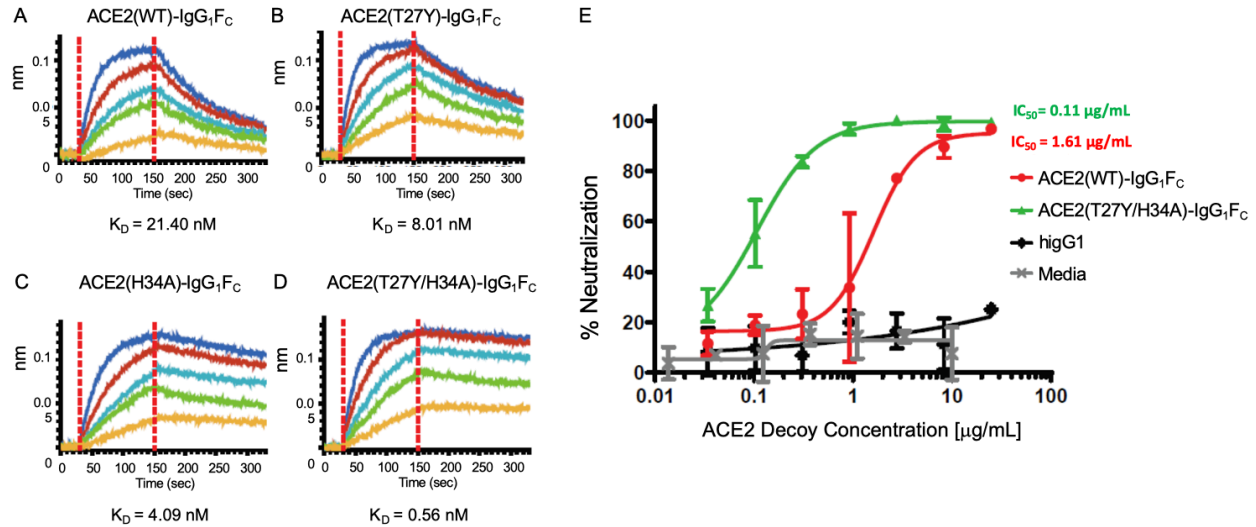
105
 106
 107 **Fig. 1** ACE2-IgG₁Fc and dimeric -IgAF_C decoys bind the spike receptor binding domain (S RBD)
 108 with high affinity. The (A) ACE2-IgG₁Fc decoy; (B) dimeric ACE2-IgAF_C decoy fused via a J-
 109 chain are shown. Bi-layer Interferometry (BLI) kinetics analysis of (C) 1:1 binding and (D)
 110 binding with avidity for the ACE2-IgG₁Fc decoy; and (E) BLI binding with avidity for the ACE2-
 111 IgAF_C decoy are shown. (F) Table of binding affinity values.

112 **An ACE2 decoy expressing T27Y and H34A mutations confers the greatest enhancement of**
113 **affinity for S RBD and improved neutralization of live SARS-CoV-2 virus *in vitro***

114 Based on MD simulation-based predictions of mutations that may confer enhanced binding
115 affinity of ACE2 for S RBD, several ACE2 variants were tested for binding affinity as ACE2-
116 IgG₁F_C fusion proteins. As shown in Figure 2, a tyrosine (Y) substitution for threonine (T) at
117 residue 27 and an alanine (A) substitution for histidine (H) at residue 34 of ACE2 resulted in 3~5
118 fold increases in binding affinities (T27Y $K_D = 8.01$; H34A $K_D = 4.09$ nM). Combination of the
119 T27Y and H34A substitutions results in a synergistic enhancement of binding affinity, showing an
120 ~35-fold increase in binding affinity as compared to ACE2(WT) with the K_D decreasing to 0.56
121 nM (Fig. 2D and F).

122 The ACE2(T27Y/H34A)-IgG₁F_C double decoy was compared to an ACE2(WT)-IgG₁F_C
123 decoy in a live SARS-CoV-2 virus assay using Vero E6 cells. As shown in Figure 2E, the double
124 mutant ACE2 decoy showed ~15-fold improvement in SARS-CoV-2 neutralization capability
125 compared to the wild type ACE2 Decoy.

126



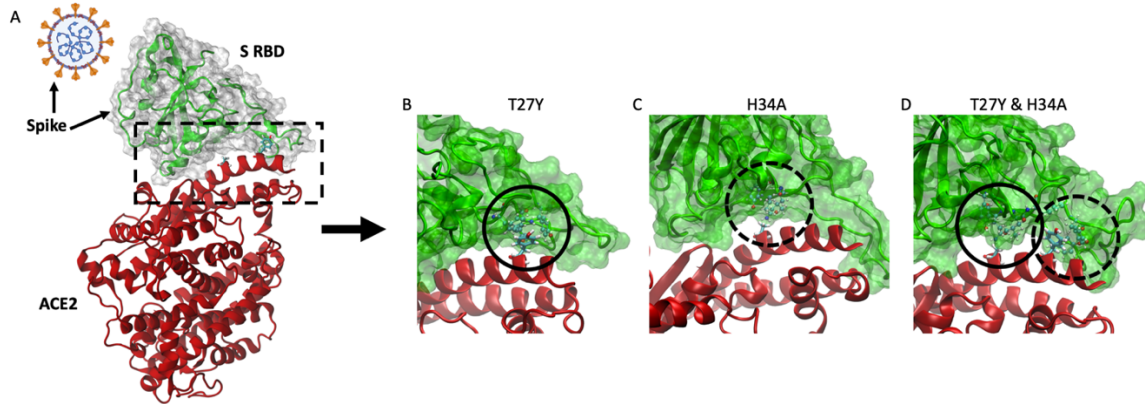
F

Decoy Sample	k_{on} (1/Ms)	k_{off} (1/s)	K_D (nM)	Virus neutralization IC_{50} (μ g/mL)
ACE2(WT)-IgG ₁ F _c	3.46E+05	7.41E-03	21.40	1.614
ACE2(T27Y)-IgG ₁ F _c	5.05E+05	4.05E-03	8.01	N/D
ACE2(H34A)-IgG ₁ F _c	2.85E+05	1.17E-03	4.09	N/D
ACE2(T27Y/H34A)-IgG ₁ F _c	3.77E+05	2.11E-04	0.56	0.107

127
 128 **Fig. 2 Biolayer Interferometry (BLI) of mutated ACE2-IgG₁F_c decoys and the live virus**
 129 **neutralization assay.** The kinetics of binding are shown for (A) ACE2(WT)-IgG₁F_c, (B)
 130 ACE2(T27Y)-IgG₁F_c, (C) ACE2(H34A)-IgG₁F_c, and (D) ACE2(T27Y/H34A)-IgG₁F_c decoys.
 131 (E) The percent neutralization over increasing concentrations (μ g/mL) of decoy is shown. (F)
 132 Binding affinity values. hlgG1 – a human IgG1 control.

133
 134 **MD simulations provide insight into greater affinity of T27Y and H34A ACE2 for S RBD**

135 MD simulations (Fig. 3) of the ACE2 T27Y and H34A substitutions suggest that a tyrosine
 136 (Y) substitution for threonine (T) at residue 27 introduces favorable hydrophobic contacts with
 137 RBD. An alanine (A) substitution for histidine (H) at residue 34 of ACE2 allows more surface area
 138 for RBD residues to contact the ACE2 helix and may favorably increase entropy by increasing
 139 side chain flexibility. Synergy between these mutations occurs since their effects are independent
 140 and do not perturb the binding pose.



141
142 **Fig. 3** *Molecular effects of T27Y and H34A ACE2 mutations predicted by MD simulation.* (A)
143 Spike (S) occurs as a trimer on the viral surface (orange projections), with the receptor binding
144 domain (RBD) being on the outermost surface. The interface between S RBD and ACE2 is within
145 the dashed box. Simulation models are shown for (B) ACE2(T27Y)- (circle), (C) ACE2(H34A)-
146 (dashed circle), and (D) ACE2(T27Y/H34A)-S RBD interactions.

147

148 **Addition of an H374N mutation inhibits ACE2 enzyme activity**

149 In addition to enhanced affinity for competitive binding of S RBD, we wanted to inhibit the
150 enzymatic activity of ACE2.²⁸ Angiotensin-converting enzyme 2 has an important role in
151 homeostasis of the renin-angiotensin system²⁹⁻³¹ by cleavage of its substrate angiotensin 1-9³²
152 and its activity affects a variety of systems. Addition of enzymatically active recombinant ACE2
153 to the system presents a high risk of unwanted side effects and since S RBD binding, but not
154 substrate cleavage activity, is the key function for the ACE2 decoy, we tested a variety of mutations
155 predicted to inhibit ACE2 enzymatic activity with a low likelihood of affecting S RBD binding
156 affinity.

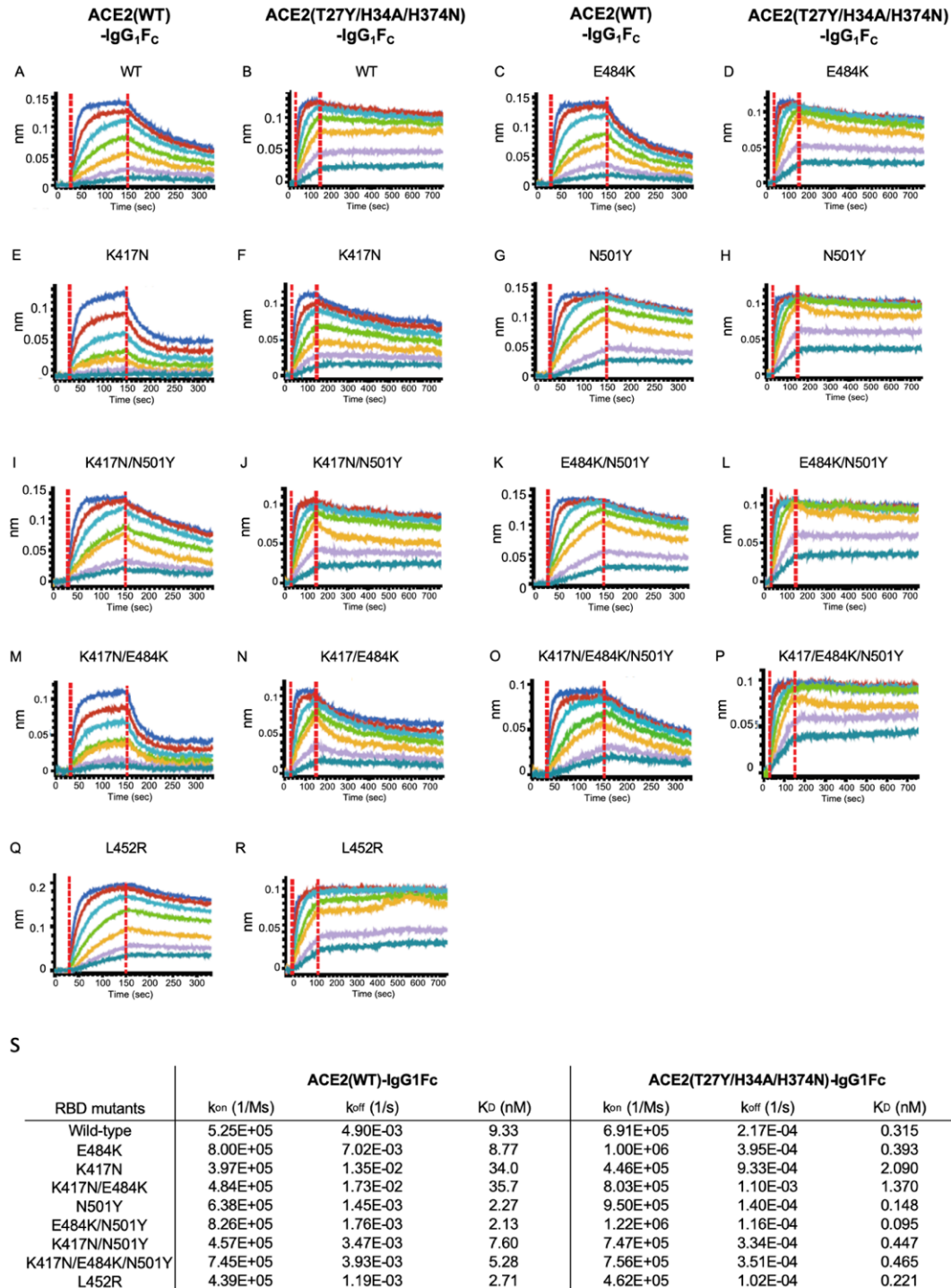
157 All of the ACE2 mutations (R273Q, R273K, R273L, H345A, H505L, H374N, or H378N)
158 predicted or known to inhibit ACE2 enzymatic activity^{33,34} did inhibit this activity in the assay
159 (Supplementary Methods, Supplementary Fig. S1). ACE2 triple mutant decoys comprising the S
160 RBD binding affinity-enhancing T27Y/H34A mutations and the enzymatic activity-inhibiting
161 mutations were produced and binding affinity assessed. Of the triple mutants, those with either the
162 R273K or H374N mutations showed the highest S RBD affinity (Supplementary Table S1).

163 The final ACE2 Triple Decoy chosen for further testing was ACE2 (T27Y/H34A/H374N)-
164 IgG₁F_C due to its more favorably biophysical characteristics as compared to an R273K-containing
165 triple mutant, including a lower propensity to aggregate and a higher titer (Supplementary Fig. S2
166 and Table S2).

167 **The ACE2 Triple Decoy shows enhanced binding to S RBD expressing N501Y and L452R**
168 **variants, with the highest affinity for S RBD expressing both N501Y and E484K**

169 The binding affinities of both the wild type ACE2 decoy (ACE2(WT)-IgG₁F_C) and the
170 ACE2(T27Y/H34A/H374N)-IgG₁F_C Triple Decoy to S RBD WT or a series of mutations found in
171 the B.1.351/P.1³⁵ (E484K/K417N/N501Y), B.1.1.7 (N501Y),^{1,26} and CAL.20.C (L452R)²⁷
172 variants are shown in Figure 4.

173 The ACE2 Triple Decoy showed higher binding affinity to all S RBD sequences as compared
174 to the wild type ACE2 decoy. As compared to the ACE2 Triple Decoy binding affinity for S RBD
175 WT, affinities for S RBD E484K/N501Y, N501Y alone and L452R were higher; affinities for S
176 RBD E484K, K417N/N501Y, N417N/E484K/N501Y, K417K/E484K, and K417N were lower.
177 Findings were similar with the wild type ACE2 decoy, with the highest affinity seen for
178 E484K/N501Y and N501Y alone, and the lowest affinities for variants expressing K417N. N501Y
179 and L452R showed ~2-3 fold increase in binding affinity for both wild type ACE2 decoy and
180 ACE2 Triple Decoy. E484K alone did not affect binding affinity to ACE2. K417N weakened
181 binding affinity for ACE2 (WT) and triple decoys, but affinity was restored when combined with
182 N501Y. The E484K, K417N and N501Y mutations occur together in the B.1.351 strain, whereas
183 L452R alone is found in CAL.20.C, therefore assessment of ACE2 WT binding to these variants
184 as they occur in nature is most physiologically relevant (Supplementary Fig. S3 and Table S3).

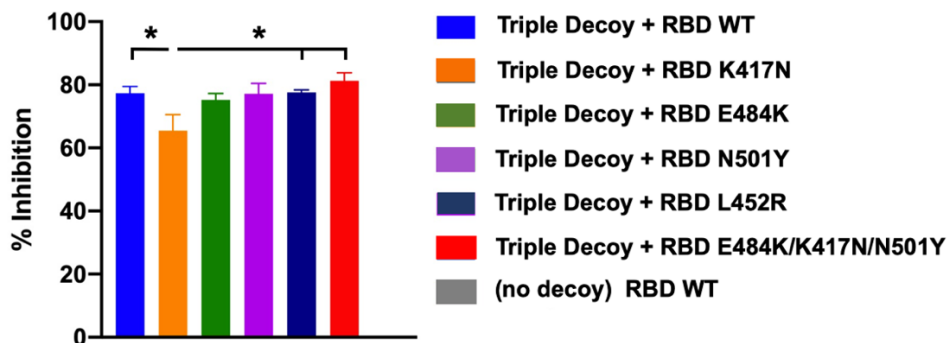


185
 186 **Fig. 4** Bi-layer Interferometry (BLI) analysis of ACE2(WT)- and ACE2(T27Y/H34A/H374N)-
 187 IgG₁F_C to spike receptor binding domain (S RBD) variants. (A-R) Comparative binding by the
 188 ACE2(WT)-IgG₁F_C or the ACE2(T27Y/H34A/H374N)-IgG₁F_C Triple Decoy to S RBD WT or a
 189 series of mutations (E484K, K417N, N501Y) alone and in combination; or S RBD with the L452R
 190 mutation are shown side-by-side (for example, ACE2(WT)IgG₁F_C versus
 191 ACE2(T27Y/H34A/H374N)-IgG₁F_C binding to S RBD WT are shown in A and B). (S) Binding
 192 affinity values.

193 **Inhibition of ACE2:S RBD binding in the surrogate virus neutralization assay correlates**
194 **with binding affinity**

195 The surrogate SARS-CoV-2 neutralization assay cPass™³⁶ is based upon assessment of
196 inhibition of binding of ACE2 (WT) to A SRB (WT). It is typically used to ascertain the presence
197 of anti-S RBD antibodies in serum. Such antibodies inhibit binding of S RBD to ACE2 bound to
198 an ELISA plate, and inhibition of greater than 20% has been reported to correlate with
199 neutralization of live virus. Here, the surrogate assay was used to determine if the ACE2 Triple
200 Decoy could inhibit S RBD WT and variant binding to plate-bound ACE2, that is, compete with
201 ACE2 (WT) for S RBD binding.

202 As shown in Figure 5, the ACE2 Triple Decoy inhibition of binding by the ACE2 Triple Decoy
203 was similar for S RBD WT, E484K, and L452R; and only slightly lower for S RBD N501Y and
204 E484K/K471N/N501Y. Only S RBD K471N binding showed a lower level of inhibition by the
205 ACE2 Triple Decoy, all other variants tested showed inhibition that was significantly higher than
206 the no-decoy control.



207 **Fig. 5** Inhibition of spike receptor binding domain (RBD) wild type (WT) and RBD variant binding
208 to ACE2 by the ACE2 Triple Decoy in the surrogate neutralization assay. The percent inhibition
209 of (competition for) RBD binding to ACE2 bound to the ELISA plate in the surrogate virus
210 neutralization assay cPass™ is shown for the ACE2 Triple Decoy with S RBD WT and the listed
211 variants. All RBD concentrations were 25 µg/mL. The negative control has no decoy. Statistics
212 performed using One-way ANOVA and Tukey's post-hoc analysis to compare Triple Decoy (but
213 not 'no decoy') binding to RBD WT and variants. For RBD K417N vs WT, $p = 0.0495$; vs L452R,
214 $p = 0.0451$; and vs E484K/K417N/N501Y, $p = 0.0128$.

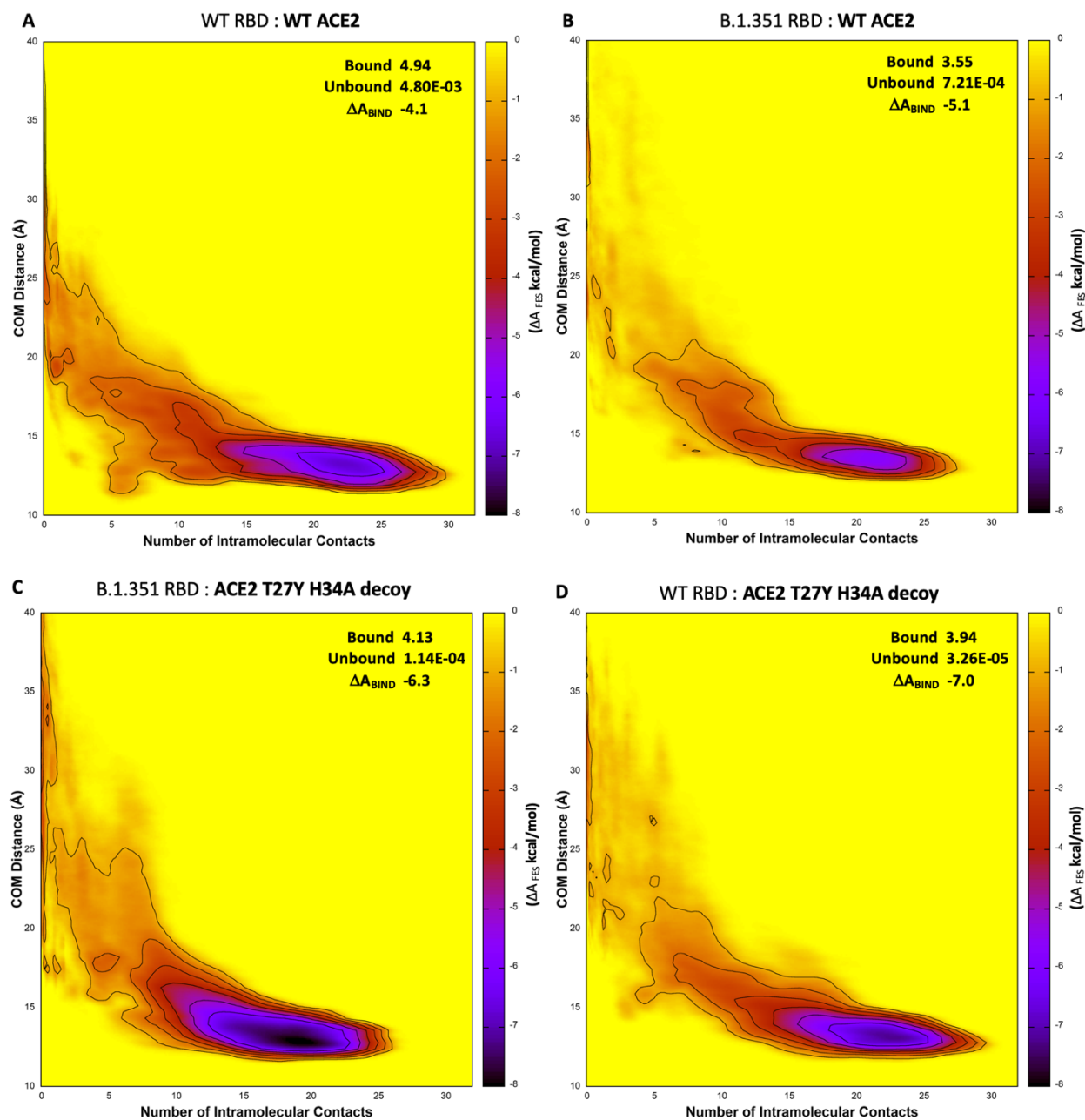
216

217 **MD simulation accurately predicts the relative affinities confirmed by *in vitro* testing**

218 We used Adaptively-Biased MD (ABMD) simulations,³⁷ which allow observation and
219 quantification of binding and unbinding, of both ACE2 WT and ACE2 (T27Y/H34A) binding to
220 S RBD WT or B.1.351 to predict binding affinities. For these simulations, the B.1.351 variant
221 comprising the E484K, K417N, and N501Y mutations was used because these mutations occur
222 together naturally and thus this combination has high physiological relevance. The ACE2
223 T27Y/H34A sequence without the additional H374N enzyme-deactivating mutation found in the
224 ACE2 Triple Decoy was used because earlier simulations had been unable to detect a change in
225 affinity due to the presence of the H374N mutation.

226 We used the Helmholtz binding free energy (ΔA_{bind}), determined by the ratio of the probability
227 of the bound and unbound states based on the Free Energy Surfaces (FES) (Figure 6), to assess
228 relative predicted affinities, where more negative values of ΔA_{bind} indicate a stronger association.
229 Details of the ABMD simulations and Helmholtz calculation can be found in *Methods*. The
230 calculated free energies of binding, in order of predicted affinity from lowest to highest, are: ACE2
231 WT:RBD WT (-4.1 kcal/mol; Fig. 6A); ACE2 WT:RBD B.1.351 (-5.1 kcal/mol; Fig. 6B); ACE2
232 T27Y/H34A:RBD B.1.351 (-6.3 kcal/mol; Fig. 6C); and ACE2 T27Y/H34A:RBD WT (-7.0
233 kcal/mol; Fig. 6D).

234 The predictive utility of these simulations is supported by the findings from the affinities (K_D)
235 determined *in vitro* and presented in Figure 4, where (for the combinations tested in MD
236 simulations) the lowest affinity was also seen for ACE2 WT : RBD WT ($K_D = 9.33$ nM), followed
237 by ACE2 WT : RBD B.1.351 ($K_D = 5.28$ nM), then ACE2 Decoy : RBD B.1.351 ($K_D = 0.465$
238 nM), and ACE2 Decoy : RBD WT ($K_D = 0.315$ nM). Note that all affinities were high, and higher
239 for Triple Decoy binding than ACE2 WT for all RBD sequences tested.



240
241 **Fig. 6.** MD simulation predicts highest affinity for the T27Y/H34A decoy to S RBD WT and
242 B.1.351. The free energy surfaces (FES) of wild type (WT) ACE2 upon interaction with (A) WT
243 RBD or (B) B.1.351 RBD; and FES for the ACE2 T27Y/H34A decoy and (C) B.1.351 RBD or
244 (D) WT RBD are shown. Darker purple represents lower free energy (ΔA_{FES} , scale at right of each
245 panel). The free energy is a function of the number of intramolecular contacts (x-axis) and the
246 distance between the centers of mass (COM, y-axis) of the interface regions.

247
248

249

250 **DISCUSSION**

251 To our knowledge, we are the first to report binding affinities of a recombinant mutant ACE2
252 decoy to the spike receptor binding domain expressing N501Y, E484K, N417Y, or L452R
253 mutations; although we note Huang *et al.* reported previously on the affinity of their ACE2-Fc to
254 S RBD with the D614G mutation.³⁸ The greater affinity of ACE2 for S RBD with the N501Y
255 substitution alone or in combination with E484K reported here is in alignment with our findings
256 in Nelson *et al.*³⁹ wherein we used MD simulation to predict that these mutations have a high
257 probability of increasing affinity for ACE2.

258 The MD simulation data presented here used to guide design of the ACE2 Triple Decoy and
259 to predict affinities of the decoy as compared to ACE2 WT for a series of variants reveal again the
260 merits of such simulations as a tool to inform therapeutic design.

261 Interestingly, widespread use of an ACE2 decoy has the potential itself to act as an
262 evolutionary force; however, an ACE2 decoy largely recognizes the same residues as endogenous
263 ACE2 and therefore it is highly unlikely a SARS-CoV-2 variant could emerge that ‘escapes’ the
264 decoy yet still binds to endogenous ACE2. This phenomenon along with limited use of a decoy
265 for therapy as compared to the spread of virus in a large population with opportunity for selection,
266 makes the decoy approach less vulnerable to loss of efficacy due to mutation of the virus.

267 The enhanced binding affinity of our Triple Mutant ACE2 Decoy to S RBD with the variant
268 mutations tested here supports continued pursuit of this therapeutic approach and further provides
269 hope that even should the efficacy of vaccines currently in distribution or therapeutic neutralizing
270 antibodies raised against WT spike be lessened by these variants, there will be an alternative
271 therapeutic approach to successfully treat COVID-19 disease.

272 In our next steps in development of the ACE2 Triple Decoy, we will address the challenge of
273 stability and successful delivery. Others developing ACE2 decoys have suggested use of intranasal
274 ⁴⁰ or nanoparticle/extracellular vesicle delivery. ^{16,41-43} We anticipate going forward into our next
275 studies using the dimeric IgA ⁴⁴ fusion protein decoy expressed by the human adenovirus serotype
276 5 E1, E2b, E3 deleted (hAd5 [E1-, E2b-, E3-]) platform that we have used successfully in our
277 vaccine development. ^{45,46} This platform can readily be used to generate oral and/or intranasal
278 formulations to further facilitate delivery. Our ACE2 Triple Decoy delivered *in vivo* using the
279 hAd5 platform is anticipated to overcome barriers to successful delivery and will be tested in
280 animal models of SARS-CoV-2 infection in future studies.

281

282 REFERENCES

- 283 1 Davies, N. G. *et al.* Estimated transmissibility and severity of novel SARS-CoV-2 Variant
284 of Concern 202012/01 in England. *medRxiv*, 2020.2012.2024.20248822,
285 doi:10.1101/2020.12.24.20248822 (2020).
- 286 2 Plante, J. A. *et al.* Spike mutation D614G alters SARS-CoV-2 fitness. *Nature*,
287 doi:10.1038/s41586-020-2895-3 (2020).
- 288 3 Hodcroft, E. B. *et al.* Emergence in late 2020 of multiple lineages of SARS-CoV-2 Spike
289 protein variants affecting amino acid position 677. *medRxiv*, 2021.2002.2012.21251658,
290 doi:10.1101/2021.02.12.21251658 (2021).
- 291 4 Weisblum, Y. *et al.* Escape from neutralizing antibodies by SARS-CoV-2 spike protein
292 variants. *Elife* **9**, e61312, doi:10.7554/eLife.61312 (2020).
- 293 5 Yu, F. *et al.* Receptor-binding domain-specific human neutralizing monoclonal antibodies
294 against SARS-CoV and SARS-CoV-2. *Signal Transduction and Targeted Therapy* **5**, 212,
295 doi:10.1038/s41392-020-00318-0 (2020).
- 296 6 Pinto, D. *et al.* Cross-neutralization of SARS-CoV-2 by a human monoclonal SARS-CoV
297 antibody. *Nature* **583**, 290-295, doi:10.1038/s41586-020-2349-y (2020).
- 298 7 Wang, Z. *et al.* mRNA vaccine-elicited antibodies to SARS-CoV-2 and circulating variants.
299 *Nature Preview*, doi:10.1038/s41586-021-03324-6 (2021).
- 300 8 Fratev, F. The N501Y and K417N mutations in the spike protein of SARS-CoV-2 alter the
301 interactions with both hACE2 and human derived antibody: A Free energy of
302 perturbation study. *bioRxiv*, 2020.2012.2023.424283, doi:10.1101/2020.12.23.424283
303 (2020).
- 304 9 Simmons, G. *et al.* Characterization of severe acute respiratory syndrome-associated
305 coronavirus (SARS-CoV) spike glycoprotein-mediated viral entry. *Proceedings of the*

- 306 *National Academy of Sciences of the United States of America* **101**, 4240-4245,
307 doi:10.1073/pnas.0306446101 (2004).
- 308 10 Li, F. Structure, Function, and Evolution of Coronavirus Spike Proteins. *Annu Rev Virol* **3**,
309 237-261, doi:10.1146/annurev-virology-110615-042301 (2016).
- 310 11 Hoffmann, M. *et al.* SARS-CoV-2 Cell Entry Depends on ACE2 and TMPRSS2 and Is
311 Blocked by a Clinically Proven Protease Inhibitor. *Cell* **181**, 271-280.e278,
312 doi:10.1016/j.cell.2020.02.052 (2020).
- 313 12 Benton, D. J. *et al.* Receptor binding and priming of the spike protein of SARS-CoV-2 for
314 membrane fusion. *Nature* **588**, 327-330, doi:10.1038/s41586-020-2772-0 (2020).
- 315 13 Greaney, A. J. *et al.* Complete Mapping of Mutations to the SARS-CoV-2 Spike Receptor-
316 Binding Domain that Escape Antibody Recognition. *Cell Host Microbe*, S1931-
317 3128(1920)30624-30627, doi:10.1016/j.chom.2020.11.007 (2020).
- 318 14 Andreano, E. *et al.* SARS-CoV-2 escape *in vitro* from a highly neutralizing COVID-19
319 convalescent plasma. *bioRxiv*, 2020.2012.2028.424451, doi:10.1101/2020.12.28.424451
320 (2020).
- 321 15 Chan, K. K. *et al.* Engineering human ACE2 to optimize binding to the spike protein of
322 SARS coronavirus 2. *Science* **369**, 1261-1265, doi:10.1126/science.abc0870 (2020).
- 323 16 Inal, J. M. Decoy ACE2-expressing extracellular vesicles that competitively bind SARS-
324 CoV-2 as a possible COVID-19 therapy. *Clin Sci (Lond)* **134**, 1301-1304,
325 doi:10.1042/cs20200623 (2020).
- 326 17 Linsky, T. W. *et al.* De novo design of potent and resilient hACE2 decoys to neutralize
327 SARS-CoV-2. *Science* **370**, 1208, doi:10.1126/science.abe0075 (2020).
- 328 18 Glasgow, A. *et al.* Engineered ACE2 receptor traps potently neutralize SARS-CoV-2.
329 *Proceedings of the National Academy of Sciences* **117**, 28046,
330 doi:10.1073/pnas.2016093117 (2020).
- 331 19 Batlle, D., Wysocki, J. & Satchell, K. Soluble angiotensin-converting enzyme 2: a potential
332 approach for coronavirus infection therapy? *Clin Sci (Lond)* **134**, 543-545,
333 doi:10.1042/cs20200163 (2020).
- 334 20 Sokolowska, M. Outsmarting SARS-CoV-2 by empowering a decoy ACE2. *Signal*
335 *Transduction and Targeted Therapy* **5**, 260, doi:10.1038/s41392-020-00370-w (2020).
- 336 21 Monteil, V. *et al.* Inhibition of SARS-CoV-2 Infections in Engineered Human Tissues Using
337 Clinical-Grade Soluble Human ACE2. *Cell* **181**, 905-913.e907,
338 doi:10.1016/j.cell.2020.04.004 (2020).
- 339 22 Nelson, G. *et al.* Millisecond-scale molecular dynamics simulation of spike RBD structure
340 reveals evolutionary adaption of SARS-CoV-2 to stably bind ACE2. *bioRxiv*,
341 2020.2012.2011.422055, doi:10.1101/2020.12.11.422055 (2020).
- 342 23 Walls, A. C. *et al.* Structure, Function, and Antigenicity of the SARS-CoV-2 Spike
343 Glycoprotein. *Cell* **181**, 281-292.e286, doi:10.1016/j.cell.2020.02.058 (2020).
- 344 24 Wrapp, D. *et al.* Cryo-EM structure of the 2019-nCoV spike in the prefusion
345 conformation. *Science* **367**, 1260-1263, doi:10.1126/science.abb2507 (2020).
- 346 25 Tegally, H. *et al.* Sixteen novel lineages of SARS-CoV-2 in South Africa. *Nature Medicine*,
347 doi:10.1038/s41591-021-01255-3 (2021).
- 348 26 Leung, K., Shum, M. H., Leung, G. M., Lam, T. T. & Wu, J. T. Early transmissibility
349 assessment of the N501Y mutant strains of SARS-CoV-2 in the United Kingdom, October

- 350 to November 2020. *Euro Surveill* **26**, doi:10.2807/1560-7917.Es.2020.26.1.2002106
351 (2021).
- 352 27 Zhang, W. *et al.* Emergence of a Novel SARS-CoV-2 Variant in Southern California. *JAMA*,
353 doi:10.1001/jama.2021.1612 (2021).
- 354 28 Liu, P., Xie, X., Gao, L. & Jin, J. Designed variants of ACE2-Fc that decouple anti-SARS-
355 CoV-2 activities from unwanted cardiovascular effects. *Int J Biol Macromol* **165**, 1626-
356 1633, doi:10.1016/j.ijbiomac.2020.10.120 (2020).
- 357 29 Warner, F. J. *et al.* Angiotensin-converting enzyme 2 (ACE2), but not ACE, is
358 preferentially localized to the apical surface of polarized kidney cells. *J Biol Chem* **280**,
359 39353-39362, doi:10.1074/jbc.M508914200 (2005).
- 360 30 Kuba, K. *et al.* A crucial role of angiotensin converting enzyme 2 (ACE2) in SARS
361 coronavirus-induced lung injury. *Nat Med* **11**, 875-879, doi:10.1038/nm1267 (2005).
- 362 31 Alifano, M., Alifano, P., Forgez, P. & Iannelli, A. Renin-angiotensin system at the heart of
363 COVID-19 pandemic. *Biochimie* **174**, 30-33, doi:10.1016/j.biochi.2020.04.008 (2020).
- 364 32 Kramkowski, K., Mogielnicki, A., Leszczynska, A. & Buczko, W. Angiotensin-(1-9), the
365 product of angiotensin I conversion in platelets, enhances arterial thrombosis in rats. *J*
366 *Physiol Pharmacol* **61**, 317-324 (2010).
- 367 33 Guy, J. L., Jackson, R. M., Jensen, H. A., Hooper, N. M. & Turner, A. J. Identification of
368 critical active-site residues in angiotensin-converting enzyme-2 (ACE2) by site-directed
369 mutagenesis. *Febs j* **272**, 3512-3520, doi:10.1111/j.1742-4658.2005.04756.x (2005).
- 370 34 Li, W. *et al.* Angiotensin-converting enzyme 2 is a functional receptor for the SARS
371 coronavirus. *Nature* **426**, 450-454, doi:10.1038/nature02145 (2003).
- 372 35 F, N. *et al.* Phylogenetic relationship of SARS-CoV-2 sequences from Amazonas with
373 emerging Brazilian variants harboring mutations E484K and N501Y in the Spike protein.
374 *virological.org (Internet)* (2021).
- 375 36 Tan, C. W. *et al.* A SARS-CoV-2 surrogate virus neutralization test based on antibody-
376 mediated blockage of ACE2-spike protein-protein interaction. *Nat Biotechnol* **38**, 1073-
377 1078, doi:10.1038/s41587-020-0631-z (2020).
- 378 37 Babin, V., Roland, C. & Sagui, C. Adaptively biased molecular dynamics for free energy
379 calculations. *J Chem Phys* **128**, 134101, doi:10.1063/1.2844595 (2008).
- 380 38 Huang, K. Y. *et al.* Humanized COVID-19 decoy antibody effectively blocks viral entry and
381 prevents SARS-CoV-2 infection. *EMBO Mol Med* **13**, e12828,
382 doi:10.15252/emmm.202012828 (2020).
- 383 39 Nelson, G. *et al.* Molecular dynamic simulation reveals E484K mutation enhances spike
384 RBD-ACE2 affinity and the combination of E484K, K417N and N501Y mutations (501Y.V2
385 variant) induces conformational change greater than N501Y mutant alone, potentially
386 resulting in an escape mutant. *bioRxiv*, 2021.2001.2013.426558,
387 doi:10.1101/2021.01.13.426558 (2021).
- 388 40 Ameratunga, R. *et al.* Inhaled modified angiotensin converting enzyme 2 (ACE2) as a
389 decoy to mitigate SARS-CoV-2 infection. *N Z Med J* **133**, 112-118 (2020).
- 390 41 Coccozza, F. *et al.* Extracellular vesicles containing ACE2 efficiently prevent infection by
391 SARS-CoV-2 Spike protein-containing virus. *J Extracell Vesicles* **10**, e12050,
392 doi:10.1002/jev2.12050 (2020).

- 393 42 Rao, L. *et al.* Decoy nanoparticles protect against COVID-19 by concurrently adsorbing
394 viruses and inflammatory cytokines. *Proceedings of the National Academy of Sciences*
395 **117**, 27141, doi:10.1073/pnas.2014352117 (2020).
- 396 43 Kim, J., Mukherjee, A., Nelson, D., Jozic, A. & Sahay, G. Rapid generation of circulating
397 and mucosal decoy ACE2 using mRNA nanotherapeutics for the potential treatment of
398 SARS-CoV-2. *bioRxiv*, doi:10.1101/2020.07.24.205583 (2020).
- 399 44 Wang, Z. *et al.* Enhanced SARS-CoV-2 neutralization by dimeric IgA. *Sci Transl Med* **13**,
400 eabf1555, doi:10.1126/scitranslmed.abf1555 (2021).
- 401 45 Rice, A. *et al.* A Next Generation Bivalent Human Ad5 COVID-19 Vaccine Delivering Both
402 Spike and Nucleocapsid Antigens Elicits Th1 Dominant CD4+, CD8+ T-cell and
403 Neutralizing Antibody Responses. *bioRxiv* <https://doi.org/10.1101/2020.07.29.227595>,
404 doi:10.1101/2020.07.29.227595 (2020).
- 405 46 Gabitzsch, E. *et al.* Complete Protection of Nasal and Lung Airways Against SARS-CoV-2
406 Challenge by Antibody Plus Th1 Dominant N- and S-Specific T-Cell Responses to
407 Subcutaneous Prime and Thermally-Stable Oral Boost Bivalent hAd5 Vaccination in an
408 NHP Study. *bioRxiv*, 2020.2012.2008.416297, doi:10.1101/2020.12.08.416297 (2021).
- 409 47 Yan, R. *et al.* Structural basis for the recognition of SARS-CoV-2 by full-length human
410 ACE2. *Science* **367**, 1444-1448, doi:10.1126/science.abb2762 (2020).
- 411 48 Maier, J. A. *et al.* ff14SB: Improving the Accuracy of Protein Side Chain and Backbone
412 Parameters from ff99SB. *J Chem Theory Comput* **11**, 3696-3713,
413 doi:10.1021/acs.jctc.5b00255 (2015).
- 414 49 Case D.A. *et al.* AMBER 2019. *University of California, San Francisco* (2019).
- 415 50 Barducci, A., Bussi, G. & Parrinello, M. Well-tempered metadynamics: a smoothly
416 converging and tunable free-energy method. *Phys Rev Lett* **100**, 020603,
417 doi:10.1103/PhysRevLett.100.020603 (2008).
- 418 51 Minoukadeh, K., Chipot, C. & Lelièvre, T. Potential of Mean Force Calculations: A
419 Multiple-Walker Adaptive Biasing Force Approach. *Journal of Chemical Theory and*
420 *Computation* **6**, 1008-1017, doi:10.1021/ct900524t (2010).

421

422 **METHODS**

423 **MD simulation**

424 *System Setup*

425 The WT-ACE2/RBD complex was built from the cryo-EM structure, PDB 6M17 of full-
426 length human ACE2 in the presence of the neutral amino acid transported B⁰AT1 with the S RBD
427 as shown in Yan *et al.* ⁴⁷ using RBD residues 336-518 and ACE2 residues 21-614. ACE2 residues
428 27 and 34 were mutated to tyrosine and alanine, respectively. The final simulation system was
429 built using the Amber ff14SB force field ⁴⁸. The RISM program from AmberTools19 ⁴⁹ was used

430 to determine optimal locations for water molecules in direct contact with the proteins. Bulk waters
431 were added to create a sufficient octahedral water box and sodium ions were added at random
432 locations to neutralize the system. After introducing mutations at the relevant residues, the same
433 procedure was used to generate the other three systems.

434 *Simulation*

435 Ten copies of each RBD/ACE2 complex were minimized, equilibrated and simulated.
436 Minimization occurred in two phases. During the first, the protein and RISM-placed waters were
437 restrained. The second phase minimized the entire system. Dynamics then began and the
438 temperature was ramped from 0 to 300K while restraining the protein and RISM-placed waters.
439 All dynamics used SHAKE restraints on hydrogen-containing bonds and a 2 fs timestep. All
440 restraints were then released and the system was equilibrated in the NPT ensemble for 2 ns. Finally,
441 each system was equilibrated in the NVT ensemble for 100 ns.

442 Steered MD was used to prepare the equilibrated systems for free energy calculation.
443 Contacting residues from the adaptively biased MD (ABMD) simulations in Nelson *et al.*^{22,37} were
444 used. Starting from the NVT equilibrated structures and over a 10 ns simulation, the number of
445 intermolecular contacts was linearly reduced to 0 using a 10 kcal/mol*Å steering bias. Structures
446 were randomly selected from the steered MD simulations and used to seed ABMD simulations.
447 Two dimensional ABMD simulations used intermolecular contacts and the center of mass distance
448 as collective variables. Centers of mass were defined as the alpha carbons from all interfacial
449 residues in each molecule. The well-tempered ABMD bias potential⁵⁰ was used for free energy
450 calculations. ABMD simulations were run for a total of 15.6μs, 16.0μs, 16.0μs and 16.38μs for
451 the ACE2 WT:RBD WT, RBD WT:ACE2 T27Y/H34A, RBD B.1.351:ACE2 WT and RBD

452 B.1.351:ACE2 T27Y/H34A, respectively. Production simulations were run in the NVT ensemble
453 meaning the calculated free energy corresponds to the Helmholtz free energy. (ΔA)

454 ABMD produces a free energy surface (FES) that describes the relative free energy between
455 any two points on the FES, ΔA_{FES} . The binding free energy (ΔA_{bind}) is determined by the ratio of
456 the probability of the bound and unbound states and can be determined from the FES:

$$457 \quad \Delta A_{\text{bind}} = -\frac{1}{\beta} \ln \frac{\int_{\text{Bound}} dx dy e^{-\beta \Delta A_{\text{FES}}(x,y)}}{\int_{\text{Unbound}} dx dy e^{-\beta \Delta A_{\text{FES}}(x,y)}} \quad (1)$$

458 Where β is the inverse of the Boltzmann constant multiplied by the temperature in Kelvins. More
459 negative values of ΔA_{bind} indicate a stronger association. The calculated ΔA_{bind} values can be
460 directly compared.

461 The “Bound” integral in equation 1 is defined to be over all $\Delta A_{\text{FES}}(x,y)$ values with the number
462 of contacts greater than 0.05 while the “Unbound” integral is over all values with fewer than 0.05
463 contacts. ΔA_{bind} was calculated with different boundaries ranging from 0.0 to 1.0, inclusive. As
464 expected, the resulting values of ΔA_{bind} changed based on the chosen boundary. However, the
465 relative ordering of the values did not. The value of 0.05 contacts was chosen as the boundary
466 because it allowed for unambiguous categorization of points as either “unbound” ($x = 0$) or
467 “partially” or “fully bound”. All simulations were performed with the GPU-enabled version of
468 pmemd from Amber20⁴⁹. Multiple-walker ABMD simulations⁵¹ used the MPI version of
469 pmemd.cuda from Amber20.

470

471 **Production of ACE2 Decoys and S RBD**

472 *Expression constructs*

473 Polymerase Chain Reactions (PCR) were conducted using PrimeSTAR GXL DNA
474 Polymerase (Takara Bio) per manufacturer's instructions. Primers and Gene Fragments were
475 synthesized by Integrated DNA Technologies (IDT). For Gibson Assembly, NEBuilder Hifi DNA
476 Assembly Master Mix (New England Biolabs) was used. For DNA ligation, we used T4 DNA
477 Ligase (NEB) per the manufacturer's instructions. Plasmid sequences were confirmed by sanger
478 sequencing (Genewiz).

479 ACE2-IgG₁FC was created by Gibson Assembly of 3 fragments: 1) the vector backbone from
480 a NheI-XhoI 7.168 kb fragment of pWT35, 2) ACE2 from a 1.86 kb PCR product of WH1043 and
481 WH1044 amplification of gene-synthesized ACE2 codon optimized for expression in CHO
482 epithelial cell line (AO615ACE2), and 3) IgG₁FC from a 0.701 kb PCR product of pXL159, using
483 primers WH1045 and WH1046. ACE2 R273Q-IgG₁FC was constructed similarly, with the
484 exception that ACE2 R273Q was created by splice by overlap extension (SOE). A 1.86 kb SOE
485 product was created by amplification with primers WH1043 and WH1044 of two PCR products:
486 1) 860 bp amplification of AO615ACE2 with primers WH1043 and WH1049, and 2) 1.059 bp
487 amplification product of AO615ACE2 with primers WH1050 and WH1044.

488 ACE2 T27Y/H34A-IgG₁FC was constructed by the Gibson Assembly of: 1) a 9.041 kb NheI-
489 PshA1 digestion fragment of ACE2-IgG₁FC plasmid, and 2) a 0.773 kb SOE product of primers
490 5MutF and 5MutR of two PCR products. The first PCR is a 0.154 kb amplification of plasmid SR9
491 with primers 5MutF and ACE2T27YR). The second PCR products is a 0.642 kb amplification of
492 plasmid SR9 with primers ACE2T27YF and 5MutR.

493 Most of the triple mutants were created by Gibson Assembly of three fragments: 1) the vector
494 backbone from a 7.168 kb NheI-XhoI fragment of pWT35, 2) IgG₁FC from a 0.701 kb PCR
495 amplification of pXL159 with primers WH1045 and WH1046, and 3) the ACE2 variant from a

496 1.86 bp PCR containing the three mutations. For the latter, the mutants were amplified with primers
497 WH1043 and WH1044 with templates pWH230 (for T27Y/H34A/R273K), pWH231
498 (T27Y/H34A/R273L), pWH236 (T27Y/H34A/H345A), pWH233 (T27Y/H34A/H505L),
499 pWH234 (T27Y/H34A/H374N), and pWH235 (T27Y/H34A/H378N).

500 ACE2 T27Y/H34A/R273Q was constructed by ligating the 9.041 bp NheI-PshA1 fragment of
501 ACE2 R273Q-IgG₁F_C and the 0.661 kb NheI-PshA1 fragment of ACE2 T27Y/H34A-IgG₁F_C.

502 *Primers (5' → 3')*:

503 5MutF GTCTTTTCTGCAGTCACCGTCACCGTCCTTG
504 5MutR TGGGTGAAGATGCTCATAGAGTGGTTTT
505 ACE2T27YF CGAGGAGCAGGCTAAATACTTTCTGGATAAGTTTAACC
506 ACE2T27YR GGTTAAACTTATCCAGAAAGTATTTAGCCTGCTCCTCG
507 WH1043 CCGTCCTTGACACGAAGCTGCTAGCGCCACCATGAGCAGCAGTAGTTGGCT
508 WH1044 GGTGGGCAAGTATGTGTTTTGTCTGCATAGGGAGACCAGTCTG
509 WH1045 AAAACACATACTTGCCACCTTGTCCTG
510 WH1046 AGTTCTAGAATCGGTATCGCTCATTTGCCAGGGCTCAGTGACAGACTC
511 WH1049 TGGTCCAGAACTGTCCCCACATG
512 WH1050 CATGTGGGGACAGTTCTGGACCA

513 *Maxcyte® transient transfection*

514 For transient expression of ACE2 decoys by Maxcyte® transfection, CHO-S cells were
515 cultured in suspension in CD-CHO media supplemented with 8 mM L-glutamine in shaker flasks
516 at 37 °C with 125 rpm rotation and 8 % CO₂. For transfection, cells in the exponential growth stage
517 were pelleted by centrifugation at 1,400 rpm for 10 min, re-suspended in 10 mL of electroporation
518 buffer, and re-pelleted at 1,400 rpm for 5 min. The cell pellet was resuspended at a density of 2 x
519 10⁸ cells/mL in electroporation buffer, mixed with the plasmid harboring either the ACE2(WT)-

520 IgG1Fc or ACE2(WT)-IgA sequence at a concentration of 150 µg/mL, and transfected using OC-
521 400 processing assemblies in a Maxcyte® ExPERT ATx Transfection System. Transfected cells
522 were incubated for 30 min at 37 °C, 5% CO₂ and then resuspended in Efficient Feed A Cocktail
523 (CHO-CD EfficientFeed™ A + 0.2% Pluronic F-68 + 1% HT Supplement + 1% L-glutamine) at
524 a density of ~4-6 x 10⁶ cells/mL. This cell culture was incubated at 37 °C with 5% CO₂ and 125
525 rpm rotation overnight, 1 mM sodium butyrate was added, and the culture was further incubated
526 at 32 °C with 3% CO₂ and 125 rpm for 13 more days; during this incubation period, Maxcyte®
527 Feed Cocktail (13.9% CD Hydrolysate, 69.5% CHO CD EfficientFeed™ A, 6.2% Glucose, 6.9%
528 FunctionMax™ Titer Enhancer, 3.5% L-Glutamine) was added at 10% of the culture volume on
529 Days 3 and Day 8.

530 *FectoPRO® transient transfection of ACE2 Mutant Decoys*

531 For transient expression of ACE2 mutant decoys by FectoPRO® transfection, CHO-S cells in
532 suspension were cultured in CD-CHO media supplemented with 8 mM L-glutamine in shaker
533 flasks at 37 °C with 125 rpm rotation and 8 % CO₂. One day before transfection, CHO-S cells were
534 seeded at a density of 1x 10⁶ cells/mL in 45 mL culture flask. On the day of transfection, 75 µL of
535 FectoPRO® transfection reagent (PolyPlus-transfection®) was mixed with 5 mL of 15 µg/mL
536 pcDNA3 plasmid DNA in CD-CHO media and incubated for 10 min at room temperature. The
537 DNA/transfection reagent mixture was added to 45 mL of CHO-S culture and incubated at 37 °C
538 with 5% CO₂ and 125 rpm rotation. On Day 3, 50 mL of the CD-CHO media supplemented with
539 8 mM L-glutamine was added and the culture incubated for an additional 4 days.

540 *Lipofectamine® transient transfection of RBD constructs*

541 For transient expression of RBD wild-type and RBD mutants, HEK-293T cells were cultured
542 and incubated at 37°C with 5% CO₂. Plasmids harboring RBD constructs were mixed with

543 lipofectamine with 1:1 (v:v) and incubated for 20 min at room temperature. The mixture was then
544 added to cultures and incubated for 3-4 days.

545 *Purification of ACE2 Decoy IgGs*

546 The MaxCyte® or FectoPRO® transfection cell culture medium was centrifuged and filtered
547 through a 0.22 µm filter to remove cells and debris, then loaded onto a HiTrap™ MabSelect
548 SuRe™ column on the AKTA Pure system pre-equilibrated with 10 mM Na Phosphate and 150
549 mM NaCl at pH 7.0. After loading, the column was washed with 10 column volumes of the same
550 buffer. The protein was eluted with 100 mM sodium acetate, pH 3.6, then immediately neutralized
551 using 2 M Tris pH 8.0. The elution fractions were pooled and dialyzed into 10 mM Hepes and 150
552 mM sodium chloride at pH 7.4.

553 *Purification of ACE2 Decoy IgAs*

554 The MaxCyte® transfection cell culture medium was centrifuged and filtered through a 0.22
555 µm filter to remove cells and debris, then loaded to a gravity column packed with CaptureSelect®
556 IgA resins (Thermo Fisher) pre-equilibrated with 10 mM Na Phosphate and 150 mM NaCl at pH
557 7.0. After loading, the column was washed with 10 column volumes of the same buffer. The protein
558 was eluted with 100 mM sodium acetate, pH 3.0, then immediately neutralized using 2 M Tris, pH
559 8.0. The elution fractions were pooled and dialyzed into 10 mM Hepes and 150 mM sodium
560 chloride, pH 7.4.

561 *Purification of RBD and RBD mutants*

562 The Lipofectamine transfection cell culture medium was centrifuged and filtered through a
563 0.22 µm filter to remove cells and debris. A buffer of 50 mM Tris, 100 mM sodium chloride, and
564 10 mM imidazole was added to the supernatant then loaded to a gravity column packed with Ni-
565 NTA resins (Qiagen) pre-equilibrated with 20 mM Tris, 300 mM sodium chloride, and 10 mM

566 imidazole, pH8.0. After loading, the column was washed with 10 column volumes of the same
567 buffer. The protein was eluted with 20 mM Tris, 150 mM sodium chloride, and 300 mM imidazole.
568 The elution fractions were pooled and dialyzed into 10 mM HEPES and 150 mM sodium chloride,
569 pH 7.4.

570 **RBD affinity determination of ACE2 decoys by Bio-Layer Interferometry (BLI)**

571 The running buffer in all experiments was 10 mM HEPES, 150 mM NaCl, pH 7.4, with 0.02%
572 tween 20, and 0.1% BSA unless otherwise indicated. For the determination of 1:1 binding affinity
573 of ACE2 Decoys against SARS-CoV2 RBD wild-type and mutants, ACE2 Decoys were
574 immobilized on an AHC sensor (Sartorius Corporation) and an RBD concentration series of 200,
575 100, 50, 25, 12.5, 6.25, 3.125 nM was used to determine the dissociation coefficient (K_D). For
576 determining ACE2 Decoy binding affinity with avidity, biotinylated RBD was immobilized on
577 streptavidin (SA) or high-precision SA (SAX) sensors, and the ACE2 Decoy concentration series
578 of 200, 100, 50, 25, 12.5, 6.25, 3.125 nM was used to determine K_D .

579 **cPass™³⁶ surrogate SARS-CoV-2 neutralization assay**

580 High BIND 96-well ELISA plates (Corning #3369) were coated with 50 ng/well ACE2 wild
581 type decoy overnight at 4°C. After the antigen solution was removed, each well was blocked with
582 150 μ L of 5% BSA/PBS for 1-2 hours at room temperature with shaking. During the blocking
583 step, 40 μ L of 50 nM RBD and RBD variants were mixed with 40 μ L of 25 μ g/mL of ACE2 decoy
584 were mixed in a 96-well plate and incubated at room temperature for 30 min with shaking. After
585 blocking, the plate was then washed 3 times with 250 μ L of PBS with 0.05% Tween 20 (PBS-T).
586 To each well, 30 μ L of 1:1667 diluted mouse anti-His, HRP and 60 μ L of RBD/ACE2 decoy (or
587 a no decoy control) were added and incubated at room temperature for 30 min. The plated was
588 washed once with 250 μ L of PBS-T. To develop the signal, 50 μ L of TMB solution was added

589 and incubated at room temperature in dark for 30 min, followed by addition of 50 μ L of 2M sulfuric
590 acid; absorbance was the read at 450nm. The percent inhibition was calculated using $(1-A_{450}$
591 $(RBD+Decoy) / A_{450} (RBD \text{ only})) \times 100$.

592

593

594

595

596

597

598

599

600

601

602

603

604

605

606

607

608

609

610

611

612

SUPPLEMENTARY MATERIAL

613 Supplementary Methods

614

615 *Assay for ACE2 enzymatic activity*

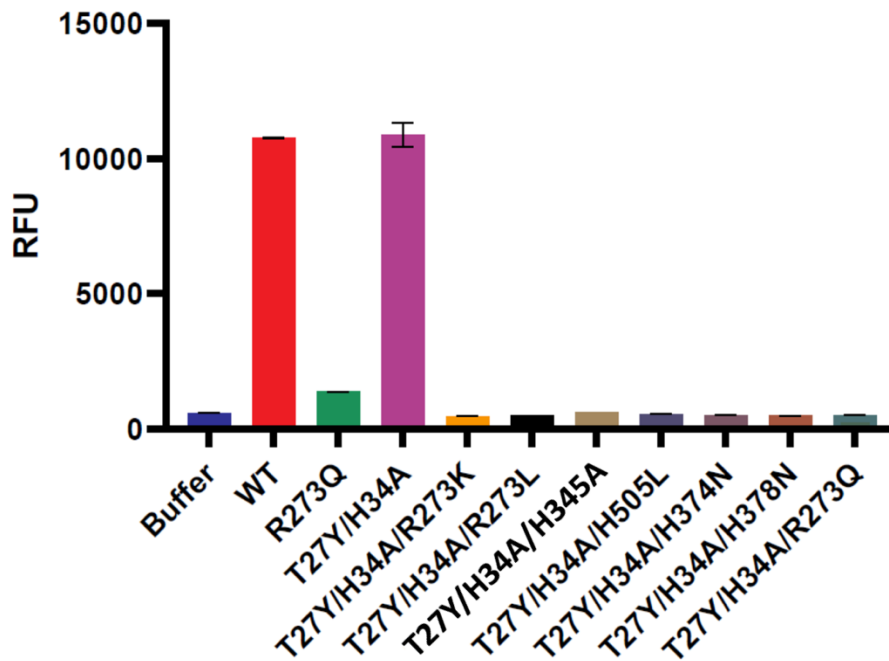
616 Enzymatic activity ACE2 decoys expressing a variety of mutations - R273Q, R273K,
617 R273L, H245A, H505L, H374N, and H378N – selected to inhibit activity in combination with
618 the S RBD affinity-enhancing mutations T27Y and H34A were assessed in the FRET based
619 ACE2 activity assay.

620

621 Supplementary Results

622

623 As shown in Figure S1, wild type (WT) and the T27Y/H34A mutations had similar ACE2
624 enzymatic activity. Addition of R273Q, R273K, R273L, H245A, H505L, H374N, or H378N
625 mutations in combination with the T27Y/H34A mutations inhibited activity of ACE2.
626



627

628 **Fig. S1.** *ACE2 activity assay.* Enzyme activity of ACE2 in relative fluorescent units (RFU) for
629 each decoy is shown.

630

631 To choose which of these activity-inhibiting mutations would be used in combination with
632 the two affinity-enhancing mutations, we compared BLI kinetic analysis of S RBD binding for
633 each. Of the triple mutants, the ones expressing R273K or H374N had the lowest dissociation
634 coefficient (K_D), that is, highest affinity binding.

635 The T27Y/H34A/H374N triple mutant was chosen for further testing because it showed
636 better biophysical properties, including a lower propensity to aggregate, higher titer/better T_m as
637 compared to the decoy with the R273K substitution.

638

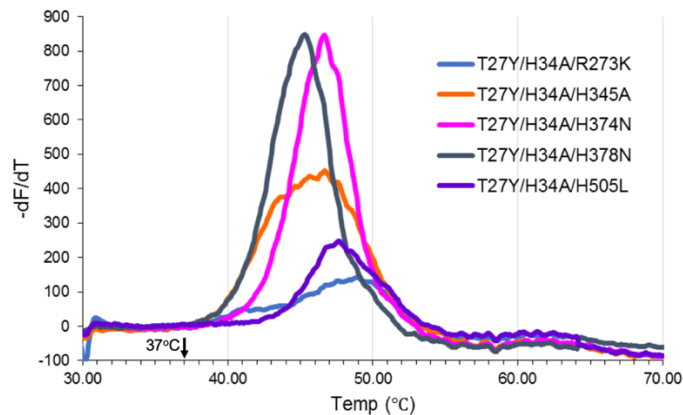
639

640 **Table S1.** BLI analysis of S RBD binding by triple mutants.

Loading Sample ID	kon (1/Ms)	koff (1/s)	KD (nM)
T27Y/H34A	3.77E+05	2.11E-04	0.56
T27Y/H34A/R273K	4.04E+05	1.79E-04	0.44
T27Y/H34A/R273L	4.06E+05	4.04E-04	1.00
T27Y/H34A/H345A	4.15E+05	3.95E-04	0.95
T27Y/H34A/H505L	4.09E+05	2.91E-04	0.71
T27Y/H34A/H374N	3.88E+05	2.44E-04	0.63
T27Y/H34A/H378N	3.95E+05	3.32E-04	0.84
T27Y/H34A/R273Q	4.86E+05	4.09E-04	0.84

641
642
643
644

Titer analysis for the triple decoys is shown below in Fig. S2 and Table S2.



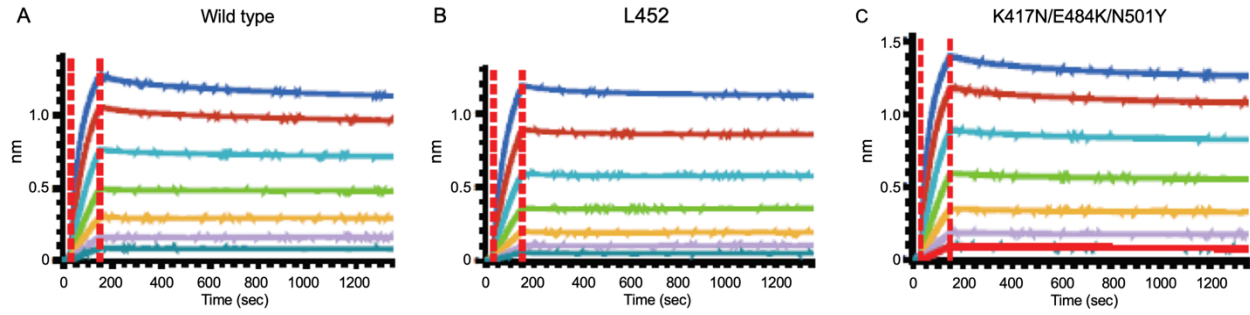
645
646 **Fig. S2.** T_m analysis

647
648 **Table S2.** T_m analysis.

ACE2 mutants	Day 7 Titer (µg/mL)	% main peak post-ProA purification
T27Y/H34A/R273K	10.6	55.7
T27Y/H34A/H345A	27.3	70.8
T27Y/H34A/H374N	23.2	82.7
T27Y/H34A/H378N	30.1	75.8
T27Y/H34A/H505A	5.3	70.0

649
650
651
652
653

The BLI kinetics analysis and binding values for ACE2 WT binding to naturally-occurring B.1.351 and CAL.20C variants are shown in Fig. S3 and Table S2.



654
655 **Fig. S3** BLI kinetic analysis of ACE wild type (WT) decoy against SARS-CoV-2 RBD WT and
656 L452R and K417N/E484K/N501Y mutants with avidity.

657
658 **Table S3.** BLI kinetic analysis of ACE(WT) decoy against SARS-CoV-2 RBD mutants with
659 avidity.

Ligand	Analyte	k_{on1} (1/Ms)	k_{on2} (1/Ms)	k_{off1} (1/s)	k_{off2} (1/s)	K_D (nM)
RBD wild-type	ACE2-IgG1Fc	1.25E+05	2.70E+00	1.38E-04	3.30E-01	1.11
RBD L452R	ACE2-IgG1Fc	8.50E+04	2.71E+00	5.03E-05	5.92E-01	0.592
RBD K417N/E484E/N501Y	ACE2-IgG1Fc	1.91E+05	2.56E+00	8.67E-05	9.62E+01	0.453

660